Research in Astron. Astrophys. **2013** Vol. **13** No. **8**, 978–990
http://www.raa-journal.org *http://www.iop.org/journals/raa*

Research in Astronomy and Astrophysics

The energetic relationship among geoeffective solar flares, associated CMEs and SEPs

Nipa J Bhatt[1], Rajmal Jain[2] and Arun Kumar Awasthi[2]

[1] Physics Dept, C. U. Shah Science College, Ashram Road, Ahmedabad – 380014, India; *nijibhatt@hotmail.com*
[2] Physical Research Laboratory (Dept. of Space, Govt. of India), Navrangpura, Ahmedabad – 380009, India; *rajmal@prl.res.in*

Received 2013 January 20; accepted 2013 April 19

Abstract Major solar eruptions (flares, coronal mass ejections (CMEs) and solar energetic particles (SEPs)) strongly influence geospace and space weather. Currently, the mechanism of their influence on space weather is not well understood and requires a detailed study of the energetic relationship among these eruptive phenomena. From this perspective, we investigate 30 flares (observed by *RHESSI*), followed by weak to strong geomagnetic storms. Spectral analysis of these flares suggests a new power-law relationship ($r \sim 0.79$) between the hard X-ray (HXR) spectral index (before flare-peak) and linear speed of the associated CME observed by LASCO/*SOHO*. For 12 flares which were followed by SEP enhancement near Earth, HXR and SEP spectral analysis reveals a new scaling law ($r \sim 0.9$) between the hardest X-ray flare spectrum and the hardest SEP spectrum. Furthermore, a strong correlation is obtained between the linear speed of the CME and the hardest spectrum of the corresponding SEP event ($r \sim 0.96$). We propose that the potentially geoeffective flare and associated CME and SEP are well-connected through a possible feedback mechanism, and should be regarded within the framework of a solar eruption. Owing to their space weather effects, these new results will help improve our current understanding of the Sun-Earth relationship, which is a major goal of research programs in heliophysics.

Key words: Sun: coronal mass ejections (CMEs) — Sun: flares — Sun: particle emission — Sun: solar-terrestrial relations — Sun: X-rays

1 INTRODUCTION

Major energetic solar eruptive events, such as filament disruption, flares and coronal mass ejections (CMEs), sometimes produce the most extreme space weather conditions in geospace and in the interplanetary medium. They produce streams of highly energetic particles known as solar energetic particles (SEPs). On impacting the Earth's magnetosphere, CME and SEP events can lead to a sudden disturbance in the Earth's magnetic field, known as a geomagnetic storm which is characterized by the disturbance storm time (Dst) index. On the other hand, both CMEs and flares may be produced by quite different mechanisms (Feynman & Hundhausen 1994) or the same mechanism but two different components of explosive magnetic-energy release (Jain et al. 2010). Currently it is not

clear whether flares or CMEs are responsible for the seed population of SEPs. Furthermore, owing to the space weather effects from flares, CMEs and SEPs, it is extremely important to understand the relationship among them, which is also a major goal of current and upcoming research programs in heliophysics.

To probe the energy release in eruptive and confined flare events, Wang & Zhang (2007) investigated X-class flares. Employing a potential field source-surface model, they found that a stronger overlying arcade field may constrain energy releases in the lower corona from being eruptive, resulting in flares without CMEs. In order to study the properties of solar source regions which have produced the fastest front side CMEs, Wang & Zhang (2008) derived a set of parameters characterizing the size, strength, morphology, complexity and free energy of active regions (ARs). Their results suggest that larger and stronger ARs with more complex magnetic configurations are more likely to produce an extremely fast CME. Similarly, Liu (2007) also concluded that the ambient magnetic field structure plays a role in determining the speed of halo CMEs. The relationship between flares and CMEs has been studied by Zhang et al. (2001), Vršnak et al. (2005), Chen & Zong (2009), Jain et al. (2010) and many other researchers. Jain et al. (2010) showed that the speed of CMEs increases with the plasma temperature of X-ray flares ($r = 0.82$). They proposed that initiation and speed of CMEs perhaps depend upon the dominant process of conversion of the magnetic field energy in the AR to heating/accelerating the coronal plasma in the reconnected loops. Aarnio et al. (2011) found that CME mass increases with flare flux. Temmer et al. (2010) found that the CME acceleration profile and the flare energy release, as evidenced in the hard X-ray (HXR) flux, evolve in a synchronized manner. However, the ultimate question still remains open: how and in what form is the flare HXR emission associated with the magnitude of CME acceleration? In the current investigation, we attempt to address this important issue.

Based on the analysis of a large sample of flare-SEP events, Jain (1986) has shown that only magnetically well-connected flares produce proton events. Kiplinger (1995) found a strong association between progressive HXR spectral hardening and interplanetary proton events. Grigis & Benz (2008) studied the spectral hardening in large solar flares and proposed that the hardening during the decay phase is caused by continued particle acceleration with longer trapping in the accelerator before escape. Grayson et al. (2009) found that flares exhibiting soft-hard-hard (SHH) behavior produced SEP events. This suggests that a flare might be a potential candidate for the seed population of SEPs produced by a long enduring reconnection process. Recently, Cliver et al. (2012) presented evidence that the difference in the slopes of the power-law size distributions of solar flares and SEP events is primarily due to the fact that SEP flares are an energetic subset of all flares. Recent reviews show that flares exhibiting SHH behavior and CMEs are both components of large eruptive flare events, which are well connected with SEP events (Kahler 2012). The nature of their connection, however, requires further quantitative understanding of their temporal, spatial as well as spectral behaviors. The role of CMEs in the generation, acceleration and prediction of energetic particles has been investigated by many researchers (Reames 1999; Tylka et al. 2005).

Recently, Li et al. (2012) discussed a "twin-CME" scenario for producing ground level enhancements (GLEs) and extreme SEP events. In this scenario, two CMEs erupt in sequence during a short period of time from the same AR with a pseudo-streamer-like pre-eruption magnetic field configuration. As a result, more diffusive shock acceleration occurs at the shock front of the second CME where particles are accelerated to high energies. Ding et al. (2013) extended this study to large SEP events in solar cycle 23 from the western hemisphere. Their findings suggest that the "twin-CME" scenario plays a very supportive role in generating large SEP events. In agreement with the "twin CME" scenario, employing multiple spacecraft observations, Shen et al. (2013) identified two eruptions resulting in twin CMEs and observed high-energy particles that led to the 2012 May 17 GLE event. Park et al. (2012) studied the dependence of SEP events on the CME parameters and found that the relationship between CME speed and SEP flux strongly depends on longitude and direction parameters. We also attempt to address the flare-CME-SEP association in the current investigation.

In this work, we analyze 30 solar flare events that are associated with CMEs in order to investigate the spectral behavior of HXRs that governs the dynamics of the CME. Furthermore, we study the spectral hardening of the flare governing the SEP energetics, and also the dependence of SEP hardness on the dynamics of the associated CME. We consider the solar flare events which were followed by geomagnetic storms of magnitude (Dst) ranging between –30 and –400 nT. Many of these events had a significant impact on geospace and space weather (Hanuise et al. 2006; Jackman et al. 2005; Barbieri & Mahmot 2004).

2 OBSERVATIONS AND DATA REDUCTION

We employ X-ray flare observations in the energy range 12–100 keV made by the Reuven Ramaty High-Energy Solar Spectroscopic Imager (*RHESSI*) (Lin et al. 2002) during the period of 2002–2006. Firstly we choose only those flares which are found to be associated with CMEs within observation limits of the Large Angle and Spectrometric Coronagraph (LASCO) onboard the *SOHO* mission. This is done by employing the technique described by Jain et al. (2010) for flare-CME association. To establish the flare-CME correlation, following Jain et al. (2010), we looked for their temporal as well as spatial association. The CMEs are detected by the LASCO coronagraphs C2 and C3, which cover a combined field of view from 2.1 to 30 R_s with a temporal cadence of around 10–50 min. Furthermore, after viewing the movies of the *GOES* soft X-ray plots in the 1–8 Å band along with the CME time lapse images made available by using composite LASCO-EIT frames named "c2eit gxray" and "c2rdif gxray," we identified if flares were associated with CMEs.

In case of non-halo CMEs, the identification was done using the central position angle (CPA) of the CME, which should coincide with the quadrant in which the flare is located. Only those flares were selected which were associated with a CME temporally as well as spatially irrespective of the heliolongitude of the flare/CME on the Sun. The solar flares were further screened based on their "geoeffectiveness" in terms of variation in the Dst index. We identify 70 events. HXR observations from *RHESSI* were available for only 40 flares due to constraints from the South Atlantic Anomaly in the *RHESSI* mission. Our next criteria to filter the selected flares are count spectra in the energy range above 50 keV. Out of 40 flares, the background supersedes above 50 keV in 10 flares. Thus, we select 30 flares for further analysis. For these flare-CME pairs, the difference between the onset time of the flares and the associated CMEs is $\pm$42 min, which is within the temporal cadence limit of the LASCO instrument. This suggests that they are well associated with each other.

Table 1 lists the characteristics of the selected 30 HXR flares, with their associated CMEs and SEPs. The flare peak time is determined in the 12–25 keV energy band. Sometimes there are two peaks with equal emission. In that case, the time of the earliest peak is considered. The *GOES* class and flare location are taken from Solar Geophysical Data reports, and details of the associated CME are taken from the LASCO catalog. The SEP/*GOES* data are obtained from *http://spidr.ngdc.noaa.gov/spidr/*. Table 1 also lists the results of the spectral analysis.

Employing an IDL routine developed for analysis of *RHESSI* data, we generate the count spectrum for each of these flares using a 1 keV wide energy bin for the energy range 12–100 keV, and 4 s time bins. The data from the front detectors in the 12–100 keV energy range are chosen. In order to maintain uniformity throughout the spectral analysis of the flare and to avoid the issues of detector cross-calibration, we use the data from detector 4 (Smith et al. 2002) for all 30 flares.

3 EXPLORING THE ENERGETIC RELATIONSHIP

3.1 Exploring the Relationship between Flares and CMEs

It has been proposed by Jain et al. (2005, 2011) that the X-ray spectrum in the energy range 1–100 keV is mainly composed of three components: the 1–12 keV soft X-ray spectrum mainly due to

Table 1 Characteristics of X-ray Flares, associated CMEs and SEPs

Flare Date and Peak Time[a] (UT)	*GOES* Class	Location	CME Onset1 Time (UT)	CME CPA	LASCO CME Speed	SEP Date and Start Time[b] (UT)	SEP Energies	F_{50}	Hardest γ	Hardest β
				(°)	(km s^{-1})		(MeV)	(Photons s^{-1} cm^{-2} keV^{-1})		
(1)	(2)	(3)	(4)	(5)	(6)	(7)	(8)	(9)	(10)	(11)
2002 Jul 23 00:35:50	X4.8	S13E72	00:27:06	HALO	2170*	…	…	…	…	…
2002 Dec 19 21:45:54	M2.7	N15W09	21:27:05	HALO	1092	...	…	…	…	…
2003 Mar 18 12:06:30	X1.5	S15W46	12:11:30	263	1601	…	…	…	…	…
2003 May 27 23:05:46	X1.3	S07W17	22:56:37	HALO	964	2003 May 28 07:00	0.8–40	2.24 ± 0.01	2.75 ± 0.019	3.01 ± 0.12
2003 May 29 01:06:06	X1.2	S06W37	00:46:03	HALO	1237	2003 May 29 06:00	0.8–40	2.53 ± 0.02	2.51 ± 0.019	2.91 ± 0.06
2003 Jun 15 23:50:50	X1.3	S07E80	23:39:40	HALO	2002*	…	…	…	…	…
2003 Jun 17 22:50:22	M6.8	S07E57	22:38:53	HALO	1813	…	…	…	…	…
2003 Oct 19 16:40:30	X1.1	N08E58	16:27:13	34	472	…	…	…	…	…
2003 Oct 22 19:59:38	M9.9	S18E78	19:43:42	93	1085	…	…	…	…	…
2003 Oct 23 19:57:54	X1.1	S21E88	19:42:43	103	1136	…	…	…	…	…
2003 Oct 24 02:49:57	M7.6	S19E72	02:34:26	113	1055	…	…	…	…	…
2003 Oct 28 11:13:33	X17.2	S16E08	11:06:20	HALO	1785*	2003 Oct 28 12:00	0.8–500	0.31 ± 0.01	2.06 ± 0.13	2.59 ± 0.03
2003 Oct 29 20:44:38	X10.0	S15W02	20:41:22	HALO	1948*	2003 Oct 29 21:00	0.8–500	3.85 ± 0.05	1.7 ± 0.018	1.71 ± 0.07
2003 Nov 02 17:18:42	X8.3	S14W56	17:19:52	HALO	1826*	2003 Nov 02 18:00	0.8–165	38.3 ± 0.1	2.7 ± 0.01	3.06 ± 0.04
2003 Nov 03 09:51:13	X3.9	N08W77	09:53:17	293	1420	…	…	…	…	…
2004 Jan 06 06:26:02	M5.8	N05E90	05:58:00	88	1469	…	…	…	…	…
2004 Jul 15 01:39:50	X1.8	S10E54	01:34:47	101	584	…	…	…	…	…
2004 Jul 22 00:30:02	M9.1	N03E17	00:44:19	184	492	…	…	…	…	…
2004 Nov 04 23:01:41	M5.4	N08E18	23:01:01	338	1055	…	…	…	…	…
2004 Nov 06 00:31:14	M9.3	N09E05	00:52:37	HALO	818	…	…	…	…	…
2004 Nov 07 16:29:02	X2.0	N09W17	16:22:12	HALO	1770*	2004 Nov 07 19:00	0.8–80	2.93 ± 0.02	2.4 ± 0.015	2.67 ± 0.05
2004 Nov 10 02:10:09	X2.5	N09W49	02:08:28	HALO	2000*	2004 Nov 10 03:00	0.8–80	7.35 ± 0.03	2.44 ± 0.01	2.63 ± 0.09
2005 Jan 01 00:29:54	X1.7	N06E34	00:21:14	HALO	832	…	…	…	…	…
2005 Jan 15 22:48:58	X2.6	N15W05	22:40:25	HALO	2861	2005 Jan 16 01:00	0.8–80	3.73 ± 0.02	2.36 ± 0.019	1.99 ± 0.09
2005 Jan 17[c] 09:47:17	X3.8	N15W25	09:43:00	HALO	2547	2005 Jan 17 12:00	0.8–165	2.18 ± 0.023	2.09 ± 0.04	2.36 ± 0.06
2005 Jan 19 08:15:02	X1.3	N15W51	08:08:30	HALO	2020	…	…	…	…	…
2005 Jan 20 06:48:17	X7.1	N14W61	06:08:58	HALO	3242*	2005 Jan 20 07:00	0.8–500	0.13 ± 0.01	2.14 ± 0.14	1.48 ± 0.02
2005 May 13 16:52:48	M8.0	N12E11	16:47:00	HALO	1689	2005 May 13 21:00	0.8–40	0.13 ± 0.003	2.85 ± 0.08	2.69 ± 0.11
2005 Jul 27 04:57:38	M3.7	N11E90	04:41:21	HALO	1787	…	…	…	…	…
2006 Dec 13 02:32:30	X3.4	S06W23	02:25:03	HALO	1774	2006 Dec 13 03:00	0.8–500	0.5 ± 0.005	2.16 ± 0.027	2.56 ± 0.05

Notes: [a] The flare peak time is determined in the 12–25 keV energy band; [b] SEP event start time (approximate) is considered by viewing plots of GOES proton flux data at five minute intervals; [c] Two CMEs occurred during the 2005 January 17 flare. The onset time of the first CME (09:06) coincides with the SXR emission of the flare. The HXR emission of the flare started at 09:35 and peaked at about 09:47:17. The onset time of the second CME (09:43) coincides with the duration of the HXR flare. Therefore, we consider the second CME to be associated with the flare (Hillaris et al. 2011). * These are the re-estimated mean plane-of-sky speeds given in the last column, denoted as "Remarks" in the LASCO CME catalog.

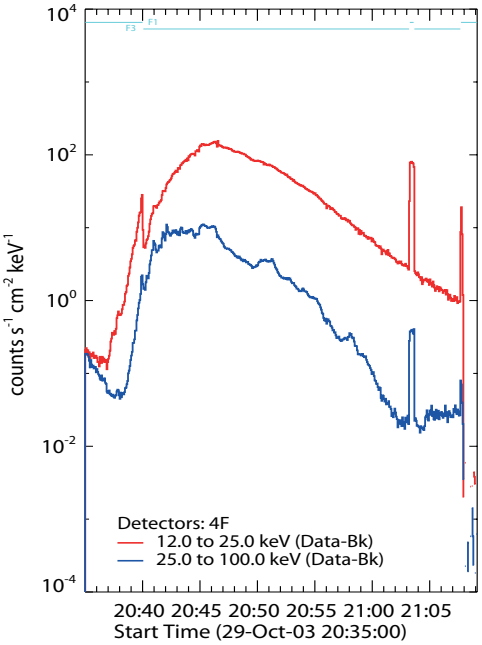

Fig. 1 Light curves of 2003 October 29 solar flare in different energy bands.

multi-thermal component; 12–25 keV emission mostly due to thermal plus non-thermal Bremsstrahlung components, and > 25 keV likely to be produced by non-thermal electrons. Thus, in order to study the non-thermal characteristics of the selected flares (cf. Table 1), we perform the spectral analysis of these flares during their rise time (about 1–2 minutes prior to flare peak time).

Figure 1 shows the light curve of the 2003 October 29 flare in the energy range of 12–25 keV (red) and 25–100 keV (blue). This flare is observed in two attenuator states A1 and A3.

The spectra are forward fitted in the energy range of 13 to 100 keV. However, before fitting the data, we correct the observed counts for pulse pileup and decimation. The lower limit of 13 keV is considered because of the instrumental effect at $\sim$11 keV (B.R. Dennis private communication). Employing the standard spectral analysis techniques for *RHESSI*, the spatially integrated count flux spectra are fitted between 13–100 keV using the combination of variable thermal (vth) and a single power law (1pow) models as shown in Figure 2(a).

Figure 2(a) shows the fitted photon spectrum with an isothermal plus single power law model. The spectral fit yields the following four free parameters: isothermal components: emission measure EM (10^{49} cm^{-3}) and plasma temperature kT (keV); non-thermal components: normalization at epivot (photon flux F_{50} of power law at 50 keV), and spectral index γ. The isothermal function also enables measurement of the relative abundance of Fe/Ni, Calcium, Sulphur and Si compared to coronal abundance. However, in the current investigation, the relative abundance is kept fixed at one. The free parameters are varied until a reasonably good fit is obtained. Systematic uncertainty is set between 0 and 0.02 so that the models fit the observed spectra with a chi-squared value ≤ 3.

In this way, we obtain γ for all 30 flares under investigation. The spectra of 29 out of 30 flares are fitted with an isothermal plus single power law model. However, in the 2003 October 28 event, we note that there is a break in the spectrum. Therefore, we fit the spectrum with the isothermal plus a broken power law model as shown in Figure 2(b). We observe that the spectrum is harder (more

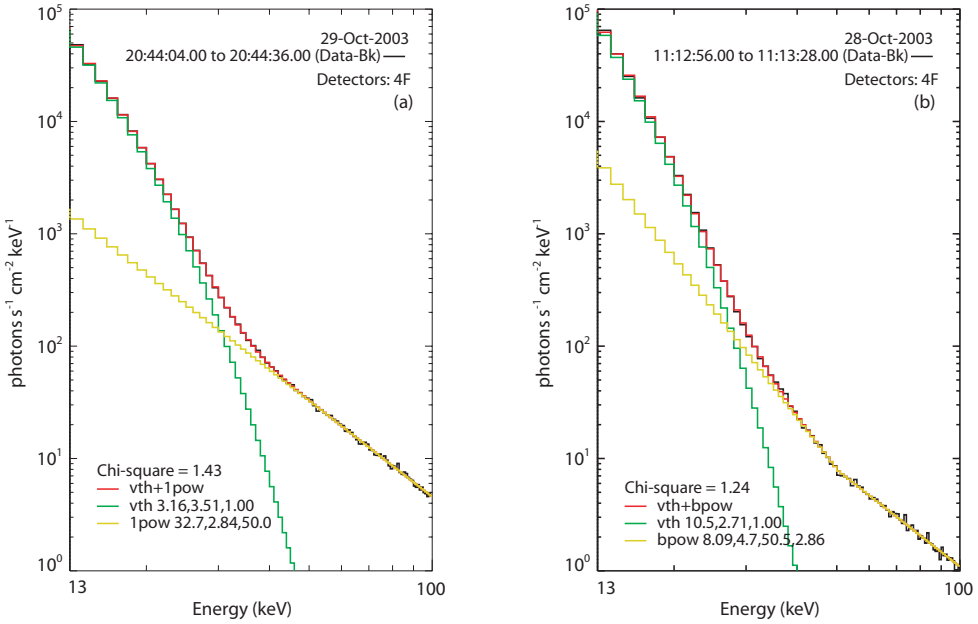

Fig. 2 Photon spectrum of 2003 October 29 (20:44:04–20:44:36 UT) is forward fitted with vth+1pow (a). Photon spectrum of 2003 October 28 (11:12:56–11:13:28 UT) is forward fitted with vth+bpow (b). Time interval: just before the peak. Energy range to fit: 13–100 keV. The fitted parameters are shown in the figure legend (*lower left corner*). In Black: observed photon spectrum; Green: vth function; Light green: 1pow in (a), and bpow in (b). Red: their total fit to the photon spectrum.

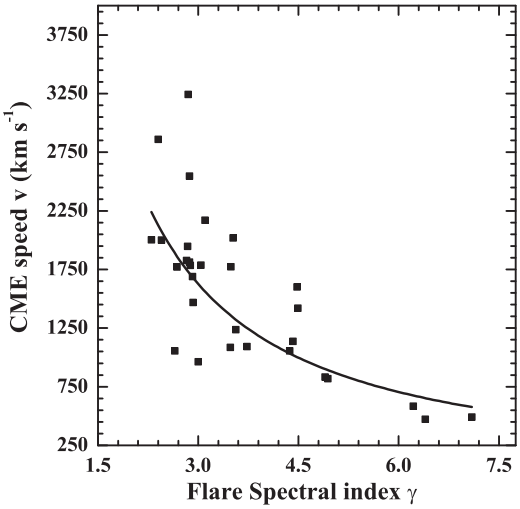

Fig. 3 Linear speed of CME v is plotted as a function of flare spectral index (before the flare peak) for 30 flares. The best fit is a power-law ($v = (6114 \pm 1503)\gamma^{-1.2\pm0.2}$) with $r \sim 0.79$.

flat) above the break energy (~ 51 keV), i.e. non-thermal, and we consider the spectral index above the break energy.

Figure 3 shows the relationship between the spectral index γ for 30 flares and the linear speed (v) of their associated CMEs. The best fit is a power-law ($v = (6114 \pm 1503)\gamma^{(-1.2\pm0.2)}$) with a correlation coefficient $\sim$0.79. This new result on the energetic relationship for flare-CME events showing association reveals that there exists a definite relationship between CME dynamics and the non-thermal characteristics (hardness) of the associated flare before the peak (in rise phase). If the spectrum of a flare during the rise phase is harder, then the associated CME has larger speed. Perhaps the flare and the associated CME occur almost simultaneously, but the observing cadence of the different instruments and their observing line-of-sight constrain simultaneous observations. For this reason, we also propose that, if the observations are not constrained, the above derived correlation coefficient may increase to ~ 1, though the magnitude of the flare and the CME may be different. Furthermore, the significant relationship between CME linear speed and the HXR γ derived during the rise phase of the flare when the reconnection is in progress suggests that the CME and the flare are the two components of one energy release system. The accelerated plasma moving down along the loops produces the X-ray flare, while plasma moving out with the magnetic field produces a CME according to the standard flare-CME model.

3.2 Exploring the Flare-SEP and CME-SEP Relationships

Investigations by Jain (1986), Kiplinger (1995), Grigis & Benz (2008) and Grayson et al. (2009) show that flare HXR emission may be a good tool for predicting SEPs. One of the issues involved in understanding the Sun-Earth relationship is the association of SEP properties with the corresponding CME event. The relationship between CMEs and SEPs has been studied by Desai et al. (2006) who propose that a CME is the cause and accelerator of the energetic particles. These studies motivated us to quantitatively explore a better relationship between the spectral characteristics of flares and associated SEPs and also between the SEP spectra and the dynamics of the associated CME.

The SEP events are determined from in situ proton temporal observations made by *GOES* in seven fixed energy channels (0.8–4, 4–9, 9–15, 15–40, 40 –80, 80–165 and 165–500 MeV). We examine the 30 flare-CME events (cf. Table 1) for their possible association with SEP enhancement near the Earth. The selection criteria for the SEP events are as follows: (i) the proton flux enhancement in all energy channels should be $\geq 5\sigma$ above the average background flux, where σ represents the standard deviation of the background proton flux. (ii) The SEP enhancement should also be observed in higher energy channels (15–40, 40–80, 80–165 and 165–500 MeV) to yield a good spectrum. This criterion is introduced in the context of the SEPs with intensity exceeding 10 pfu in the energy channels $>$10 MeV that have a significant impact on space weather (Gopalswamy 2010). We find that only 12 events out of the 30 flare-CME events satisfy the above criteria, and are listed in Table 1 (column 7). It is interesting to note that the 12 qualifying events occurred between longitudes 11°E–61°W. This is within the range of heliolongitude proposed earlier by Jain (1986). He proposed that a two-ribbon flare with associated CME launched in the longitude zones of 30°E–70°W from the Sun is a good carrier of accelerated energetic particles that propagate along the curved Parker spiral interplanetary magnetic field lines and thereby are likely to reach the Earth.

3.2.1 Flare spectral analysis

In this section, we study the X-ray spectra for the whole observed duration of each flare event to probe the temporal evolution of the spectral index (γ) in the energy range of 50–100 keV. We ensure that an attenuator does not change during the selected time interval required to form the spectra. The selection of the subintervals to form the spectra is determined on the basis of count statistics. The subintervals should be long enough to provide sufficient counts and short enough to show the expected variations in the spectra with flare evolution. In order to make judicious spectra in the

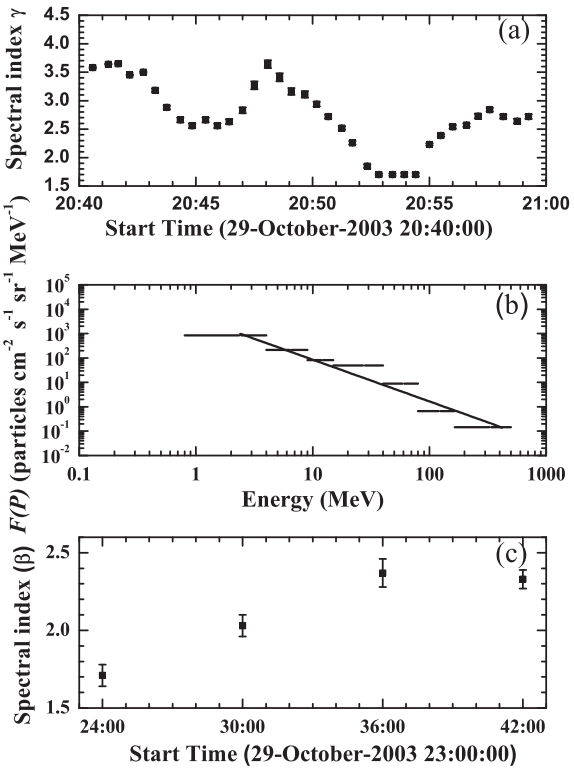

Fig. 4 (a) Temporal evolution of flare spectral index $\gamma \pm \sigma$ of 2003 October 29 in the energy range 50–100 keV. Hardest $\gamma \pm \sigma = 1.7 \pm 0.018$; the error bars are obtained while fitting the spectra in OSPEX, showing the limits. (b) Background-subtracted proton spectrum for the interval 2003 October 30 00:00–06:00 UT fitted with a power law in the energy range of 0.8–500 MeV. (c) Temporal evolution of proton spectral index β from the 2003 October 29 proton event in the energy range 0.8–500 MeV. Hardest $\beta = 1.71 \pm 0.07$.

energy range 50–100 keV, the spectra are formed for the subinterval duration of 16 s to 32 s (i.e. in multiples of 4 s time bins – the spacecraft spin period) to optimize count flux statistics, which would yield better spectral fits. The non-thermal hard X-ray energy range is determined individually for each spectral interval before fitting by the signal-to-noise (S/N) ratio to guarantee that the signal does not mix with the background. We consider the forward fitting method and carry out spectral fitting in the energy range 13 to 100 keV, however, depending upon the goodness of the S/N ratio. The spatially integrated count flux spectra are fitted considering a combination of an isothermal component and a single power law model as described earlier in Section 3.1. Like earlier, the majority of flares are best fitted with an isothermal plus single power law model, but there are exceptions in some flares for a few time intervals, and we employ a broken power law fit (as shown in Fig. 2(b)). In such cases the spectral index above the break energy is considered for investigation. The optimum values of the parameters are determined through iterative fitting and chi-squared minimization. We varied the free parameters for each spectral interval to achieve the best fit (chi-squared value ≤ 3) between the model and the observed spectra. For each spectrum, we derived a value of the spectral index $\gamma \pm \sigma$, where σ is the error estimate (showing the limits/uncertainty) obtained while fitting the spectra in OSPEX.

Figure 4(a) shows the temporal evolution of spectral index $\gamma \pm \sigma$ in the energy range 50–100 keV for the 2003 October 29 flare. We perform the spectral analysis for all 12 flares that show a relationship with SEPs, as listed in Table 1. The photon flux at 50 keV (F_{50}) and the hardest spectral index $\gamma \pm \sigma$ revealed from the hardest spectrum of each individual flare are listed in Table 1. We observe that out of these 12 flare events, the 2003 October 29 event gives the hardest $\gamma \pm \sigma$, which is equal to 1.7 ± 0.018 and a corresponding $F_{50} \sim 3.85 \pm 0.05$ (photons s^{-1} cm^{-2} keV^{-1}). It is interesting to note that out of these 12 events, the strongest geomagnetic storm of cycle 23 was produced by the 2003 October 29 event (Dst ~ -383 nT), which had a significant impact on space weather.

3.2.2 SEP spectral analysis

We perform the spectral fit on the proton spectra generated in the energy range 0.8–500 MeV for each of the 12 SEP events observed after the flare onset. The proton spectra are formed from the proton flux measurement made by the *GOES*-8/*GOES*-11 satellites. We accumulate the proton data integrated over 6 h starting from the SEP onset time to the next 18–24 h.

Figure 4(b) shows the spectrum for the interval 2003 October 30 00:00–06:00 UT associated with the 2003 October 29 event fitted between 0.8–500 MeV with a power law. From the spectral fit we derive power law spectral index β. We carry out the spectral fit for each 6 h interval and measure β for that interval. Figure 4(c) shows the temporal evolution of β for the 2003 October 29 proton event in the energy range 0.8 to 500 MeV. For a given proton event, we consider the hardest (most flat) spectra observed in the event for a further relationship with the hardest flare spectra.

3.2.3 Flare-SEP and CME-SEP relationship

In order to investigate the relationship between flares and SEPs, as discussed in Section 3.2.1, we study the HXR spectra for the whole observed duration of all the SEP related flares. Having obtained the temporal evolution of the spectral index (γ) in the energy range 50–100 keV, we consider the hardest spectral index (γ) for these flares. Similarly, as discussed in Section 3.2.2, we study the temporal evolution of β for all the 12 proton events. For a further investigation, we consider the hardest spectral index β for all the 12 SEP events. Shown in Figure 5 is a plot of the hardest X-ray spectral index γ of the solar flare as a function of the hardest spectral index β of the associated proton event for all 12 flare-SEP events. We find a strong linear correlation ($r \sim 0.9$) between γ and β representing the empirical relation $\gamma = (0.61 \pm 0.01)\beta + (0.82 \pm 0.03)$.

Figure 5 shows the 99% confidence level (dotted line) of the best fit (solid line). The strong linear relationship between γ and β reveals that the flare site may be the origin of protons observed near the Earth. This also suggests that the primary acceleration of SEPs to higher energies occurs at the flare site.

To study the CME-SEP connection, we investigate the spectral behavior (hardness parameter β) of an SEP event and its relation with the dynamics of the associated CME. Figure 6 shows the hardest proton spectral index β as a function of associated CME linear speed v for all the 12 SEP events. However, the 2003 October 29 event seems to be an outlier and hence, the fit was done for the remaining 11 events. The best fit is a power law ($\beta = 2.94 - (6.8 \times 10^{-12})v^{3.23}$) with a correlation coefficient of ~ 0.96.

Figure 6 shows the 99% confidence level (dotted line) of the best fit (solid line). The strong power-law relationship of hardest β with CME speed reveals that the CMEs may play a significant role in the acceleration of the SEPs. The larger the CME speed is, the harder the corresponding SEP event is. The seed population of the low energy protons (< 5 MeV) is perhaps triggered during the reconnection time when a flare and a CME also occur which, however, is further carried and accelerated by CME driven shocks during their passage towards the Earth. Thus, secondary acceleration of SEPs takes place on their way to the Earth due to the CME driven shocks. The largest correla-

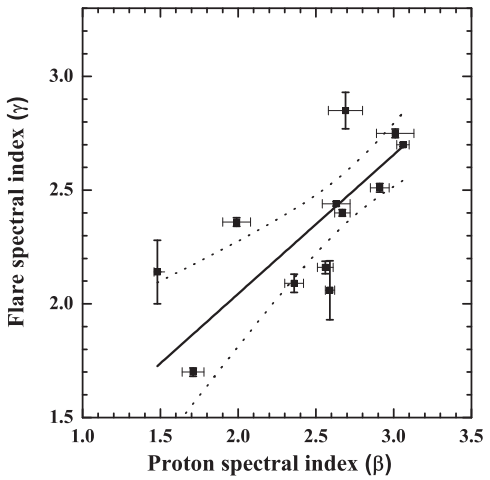

Fig. 5 Flare spectral index γ (hardest) as a function of the hardest proton spectral index β. The solid line is the best fit ($\gamma = (0.61 \pm 0.01)\beta + (0.82 \pm 0.03)$) with a correlation coefficient of ~ 0.9. The two dotted lines denote a 99% confidence level of the best fit.

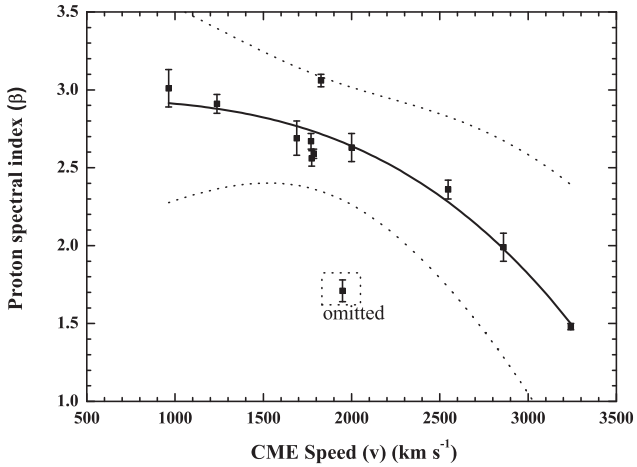

Fig. 6 Hardest proton spectral index β as a function of CME linear speed v. The solid line is the best fit ($\beta = 2.94 - (6.8 \times 10^{-12})v^{3.23}$) with a correlation coefficient of ~ 0.96. The two dotted lines denote a 99% confidence level of the best fit.

tion appears between CME speed and β, suggesting that the "secondary" acceleration is even more important than the "primary" acceleration that occurs at the flare-CME onset.

These newly discovered scaling laws have an important implication in the context of space weather research in that HXR spectra of the flare and the CME speed may both be employed to predict the degree of spectral hardness/strength of SEPs, which arrive near the Earth in < 10 h and affect the geospace environment in a variety of ways. However, this conclusion is in contrast to Gopalswamy et al. (2004) who proposed a poor relationship between the proton intensity of SEP

events and X-ray flare size. Combining the results of our observations (Figs. 5 and 6), we propose that the particles are primarily accelerated at the flare site and secondary acceleration takes place on their way to the Earth due to shocks produced by the CME. We propose that combining our new results with Jain (1986) would make it easier to predict the geoeffectiveness of a flare as well as the degree of spectral hardness/strength of the associated SEP event.

4 DISCUSSION AND CONCLUSIONS

The aims of this paper can be put into the following key questions: Are flare and/or CME events responsible for seed population and acceleration of the SEPs? How and in what form is flare HXR emission associated with the magnitude of CME acceleration? Do flares, CMEs and acceleration of SEPs all occur at the reconnection site in the corona? In order to address these questions, we analyzed the HXR spectra of 30 solar flare events and cross correlated them with the linear speed of the associated CMEs. Furthermore, out of 30 flare events, 12 events were chosen to explore their flare-SEP and CME-SEP relationships. Our three important results are as follows.

(1) Flare-CME relationship: a good power-law relationship ($r \sim 0.79$) is observed between the non-thermal HXR spectral index (γ) (during the rise phase of flare) and the CME linear speed (v). This suggests that a flare and the associated CME are the two components of one energy release system and perhaps occur nearly simultaneously during the impulsive acceleration at the reconnection site. This new result on the energetic relationship for events where the flare and CME are associated reveals that there exists a definite relationship between CME dynamics and the non-thermal characteristics (hardness) of the associated flare before the peak (in rise phase).
(2) Flare-SEP relationship: we find a strong linear relationship between the hardest X-ray spectral index of the flare (γ) and the hardest spectral index (β) of the associated high energy protons ($r \sim 0.9$). This relationship reveals that the flare site may be the origin of protons observed near the Earth and it also favors the idea that the primary acceleration of SEPs to higher energies occurs at flare sites.
(3) CME-SEP relationship: a strong power-law relationship ($r \sim 0.96$) is observed between the hardest proton spectral index β and the associated CME linear speed v for 11 CME-SEP events (the 2003 October 29 event seems to be an outlier). This study reveals that on their way to the Earth, the CMEs may play a significant role in the secondary acceleration of the SEPs. The larger the CME speed is, the harder the corresponding SEP event is. The largest correlation appears between CME speed and β, suggesting that the "secondary" acceleration by the CME driven shock is even more important than the "primary" acceleration, which, however, occurs during the flare-CME trigger at the reconnection site. We propose that the particles are primarily accelerated at the flare site and secondary acceleration takes place on their way to the Earth due to shocks produced by the CME.

Integrating all the three results we conclude that all three solar eruptive phenomena (flares, CMEs and SEPs) are the components of one energy release system. However, if the CME carrying the enhanced SEP material is well connected with field lines to the Earth then it may affect the geospace environment (Jain 1986).

On the other hand, in the context of acceleration of CMEs our results contradict those from Maričić et al. (2007). They found that the reconnection rate is more relevant for the CME acceleration than a strong heating and non-thermal particle acceleration. Our study shows the relationship between the flare spectral index (non-thermal) during the rise phase of the flare and the CME linear speed, supporting the "standard" flare/CME model which predicts a relationship between the energy release process in a flare and the dynamics of the associated CME (e.g. Lin 2004). Our investigations show that linear speed of the CME is well-coupled with the non-thermal flare emission during the rise phase of the flares (when the reconnection occurs) as well as the hardness of SEPs.

The results from the present study provide strong evidence for the association among the HXR non-thermal flare emission, the CME dynamics and SEP acceleration, and suggest that they are all components of one energy release system. The results in Section 3.2.3 suggest that both the hardest spectral parameter from the flare (non-thermal) and the associated speed of the CME play a key role in deciding the degree of spectral hardness/strength in an SEP event near the Earth. We propose that this novel work may be extended for a better prediction of SEP events. We also propose that quantitative study of this nature may lead to developing a prediction tool for the degree of spectral hardness/strength of the SEP events. The derived relationship among flares, CMEs and SEPs suggests that there exists a close physical connection among solar eruptive phenomena, which can significantly impact space weather.

In order to study solar eruptive phenomena, various current space missions, viz. *SOHO*, *WIND*, *ACE*, *RHESSI*, *HINODE*, *STEREO* and *SDO*, are in operation, which have revolutionized solar-terrestrial physics research. We believe that our current investigations, employing observations from current missions, will further help in the present understanding of space weather and space climate as well as the relationship between Sun and Earth. We further propose to consider the outcome of the present investigation in the focal topics of proposed future space missions, viz. Solar Probe Plus, Solar Orbiter, Solar Eruptive Events (SEE) (Lin 2011) etc., which may allow studying the various fundamental processes of energy release in solar eruptive events and their influence on Earth and in interplanetary space.

Acknowledgements We are extremely thankful to Professors Brian. R. Dennis and Markus. J. Aschwanden for their valuable suggestions. We sincerely acknowledge our thanks to the anonymous referee for his/her valuable suggestions that improved the paper. HXR flare data from *RHESSI*, CME data from LASCO/*SOHO* and SEP data from *GOES* missions are duly acknowledged. This work is carried out under the CAWSES-India Program, supported by the Indian Space Research Organization (ISRO), Dept. of Space, Govt. of India.

References

Aarnio, A. N., Stassun, K. G., Hughes, W. J., & McGregor, S. L. 2011, Sol. Phys., 268, 195
Barbieri, L. P., & Mahmot, R. E. 2004, Space Weather, 2, S09002
Chen, A.-Q., & Zong, W.-G. 2009, RAA (Research in Astronomy and Astrophysics), 9, 470
Cliver, E. W., Ling, A. G., Belov, A., & Yashiro, S. 2012, ApJ, 756, L29
Desai, M. I., Mason, G. M., Mazur, J. E., & Dwyer, J. R. 2006, Space Sci. Rev., 124, 261
Ding, L., Jiang, Y., Zhao, L., & Li, G. 2013, ApJ, 763, 30
Feynman, J., & Hundhausen, A. J. 1994, J. Geophys. Res., 99, 8451
Gopalswamy, N., Yashiro, S., Krucker, S., Stenborg, G., & Howard, R. A. 2004, Journal of Geophysical Research (Space Physics), 109, A12105
Gopalswamy, N. 2010, in 20th National Solar Physics Meeting, ed. I. Dorotovic, 108
Grayson, J. A., Krucker, S., & Lin, R. P. 2009, ApJ, 707, 1588
Grigis, P. C., & Benz, A. O. 2008, ApJ, 683, 1180
Hanuise, C., Cerisier, J. C., Auchère, F., et al. 2006, Annales Geophysicae, 24, 129
Hillaris, A., Malandraki, O., Klein, K.-L., et al. 2011, Sol. Phys., 273, 493
Jackman, C. H., Deland, M. T., Labow, G. J., et al. 2005, Journal of Geophysical Research (Space Physics), 110, A09S27
Jain, R. 1986, MNRAS, 223, 877
Jain, R., Dave, H., Shah, A. B., et al. 2005, Sol. Phys., 227, 89
Jain, R., Aggarwal, M., & Kulkarni, P. 2010, RAA (Research in Astronomy and Astrophysics), 10, 473
Jain, R., Awasthi, A. K., Chandel, B., et al. 2011, Sol. Phys., 271, 57
Kahler, S. W. 2012, ApJ, 747, 66

Kiplinger, A. L. 1995, ApJ, 453, 973
Li, G., Moore, R., Mewaldt, R. A., Zhao, L., & Labrador, A. W. 2012, Space Sci. Rev., 171, 141
Lin, J. 2004, Sol. Phys., 219, 169
Lin, R. P. 2011, Space Sci. Rev., 159, 421
Lin, R. P., Dennis, B. R., Hurford, G. J., et al. 2002, Sol. Phys., 210, 3
Liu, Y. 2007, ApJ, 654, L171
Maričić, D., Vršnak, B., Stanger, A. L., et al. 2007, Sol. Phys., 241, 99
Park, J., Moon, Y.-J., & Gopalswamy, N. 2012, Journal of Geophysical Research (Space Physics), 117, A08108
Reames, D. V. 1999, Space Sci. Rev., 90, 413
Shen, C., Li, G., Kong, X., et al. 2013, ApJ, 763, 114
Smith, D. M., Lin, R. P., Turin, P., et al. 2002, Sol. Phys., 210, 33
Temmer, M., Veronig, A. M., Kontar, E. P., Krucker, S., & Vršnak, B. 2010, ApJ, 712, 1410
Tylka, A. J., Cohen, C. M. S., Dietrich, W. F., et al. 2005, ApJ, 625, 474
Vršnak, B., Sudar, D., & Ruždjak, D. 2005, A&A, 435, 1149
Wang, Y., & Zhang, J. 2007, ApJ, 665, 1428
Wang, Y., & Zhang, J. 2008, ApJ, 680, 1516
Zhang, J., Dere, K. P., Howard, R. A., Kundu, M. R., & White, S. M. 2001, ApJ, 559, 452